Available online at www.sciencedirect.com
ScienceDirect
Journal of Sound and Vibration 321 (2009) 554–571
JOURNAL OF SOUND AND VIBRATION
www.elsevier.com/locate/jsvi

Dynamic response and stability analysis of an unbalanced flexible rotating shaft equipped with *n* automatic ball-balancers

J. Ehyaei*, Majid M. Moghaddam

Department of Mechanical Engineering, Tarbiat Modares University, Tehran, Iran

Received 2 July 2008; received in revised form 13 October 2008; accepted 13 October 2008
Handling Editor: M.P. Cartmell
Available online 30 November 2008

Abstract

The paper presents analytical and numerical investigations of a system of unbalanced flexible rotating shaft equipped with *n* automatic ball-balancers, where the unbalanced masses are distributed in the length of the shaft. It includes the derivation of the equations of motion, the stability analysis on the basis of linearized equations of motion around the equilibrium position, and the results of the time responses of the system. The Stodola–Green rotor model, of which the shaft is assumed flexible, is proposed for the analysis step. The rotor model includes the influence of rigid-body rotations, due to the shaft flexibility. Utilizing Lagrange's method, the nonlinear equations of motion are derived. The study shows that for the angular velocities more than the first natural frequency and selecting the suitable values for the parameters of the automatic ball-balancers, which are in the stability region, the auto ball-balancers tend to improve the vibration behavior of the system, i.e., the partial balancing, but the complete balancing was achieved in a special case, where the imbalances are in the planes of the auto ball-balancers. Furthermore, it is shown that if the auto ball-balancers are closer to the unbalanced masses, a better vibration reduction is achieved.

1. Introduction

Imbalance in rotating machines is a common source of the vibration excitation. For a rotor with a constant unbalanced mass, only one-time balancing is sufficient. However, if the rotor has variable unbalanced mass depending on the running conditions, balancing of the rotor cannot be achieved by only one-time balancing. For this reason, automatic ball-balancer (ABB) is used to reduce the unbalancing effects in rotating machines, such as washing machines, turning lathes, etc. ABB is a device for eliminating the variable imbalance of rotating machines automatically. It is usually composed of a circular disk with a groove, or race, containing spherical or cylindrical weights and a low viscosity damping fluid.

Many researches have been conducted in the field of auto balancers since 1930 but they have not been so remarkable relative to other balancing topics. Initial researches were established by Thearl [1,2], Alexander [3] and Cade [4]. Experimental and analytical analysis of auto balancers for non-autonomous systems can be found in Refs. [5–7]. Chung and Ro [8] studied the stability and dynamic behavior of an ABB for the Jeffcott

*Corresponding author.
E-mail address: jehyaei@gmail.com (J. Ehyaei).

0022-460X/$ - see front matter © 2008 Elsevier Ltd. All rights reserved.
doi:10.1016/j.jsv.2008.10.019

rotor. They consider an autonomous system by utilizing the polar coordinate system, and so they did the stability analysis in a better way relative to the previous researches. Hwang and Chung [9] applied this approach to an ABB with double races. Sperling and his co-workers considered the analytical and numerical investigations of a two-plane automatic balancing device for equilibration of rigid-rotor imbalance [10]. Chung and Jang studied the dynamic stability and the time responses for an ABB of a rotor with a flexible shaft. They utilized the Stodola–Green rotor model, of which the shaft is flexible; their model was able to include the influence of rigid-body rotations due to the shaft flexibility [11]. Chao, Huang and Sung presented the non-planar dynamic modeling and analysis of the spindle–disk system equipped with an automatic ball-type balancer system for optical disk drives [12]. In another paper, Yang and his co-workers investigated the influence of friction in an automatic ball balancing system [13].

Kim, Lee and Chung analyzed the dynamic behavior and stability of an ABB in an optical disk drive based on the proposed three-dimensional dynamic model [14]. Rajalingham and Bhat investigated the suitability of a two-ball automatic balancer to balance the residual unbalance in a vertical rotor [15]. Green, Champneys and Lieven presented a nonlinear bifurcation analysis of the dynamics of an automatic dynamic balancing mechanism for rotating machines [16]. Lu and Hung studied the dynamic characteristics of a three-ball automatic balancer and considered the effects of the number of balls on the stability of the system [17]. Cheng and his co-workers proposed a novel design of a vibration absorber for reducing the vibration caused by the imbalance of an optical disk drive. They designed and analyzed the auto balancer of an optical disk drive using speed-dependent vibration absorbers [18]. Rodrigues and his co-workers presented an analysis of a two-plane automatic balancing device for rigid rotors [19].

In this study, the stability and time responses for a system of unbalanced flexible rotating shaft equipped with n ABBs, where the unbalanced masses are distributed in the length of the shaft are analyzed. It must be noted that in almost all the previous researches the rotor model is Jeffcott. Since the Jeffcott rotor model is basically a particle or point–mass representation, this model is inadequate to explain rigid-body characteristics caused by the flexibility of a rotor shaft [20]. Therefore, in order to analyze the dynamics of the system, the Stodola–Green rotor model [21,22] is adopted instead of the Jeffcott model. Also, in this research, auto ball balancing in multiplane is considered despite other studies whose focus has been on single plane balancing.

2. Nonlinear equations of motion

The Stodola–Green rotor model with n ABBs is shown in Figs. 1 and 2, where the flexible rotor is installed on two elastic supports. It is assumed that the shaft mass is negligible compared to the mass of other elements and the shaft is slender. The slender beam implies that the Euler–Bernoulli beam theory is applied when driving the equations of motion. Furthermore, the internal damping of the shaft is relatively smaller than the damping in the bearings, and so it can be neglected. The XYZ coordinate system is a space fixed inertia

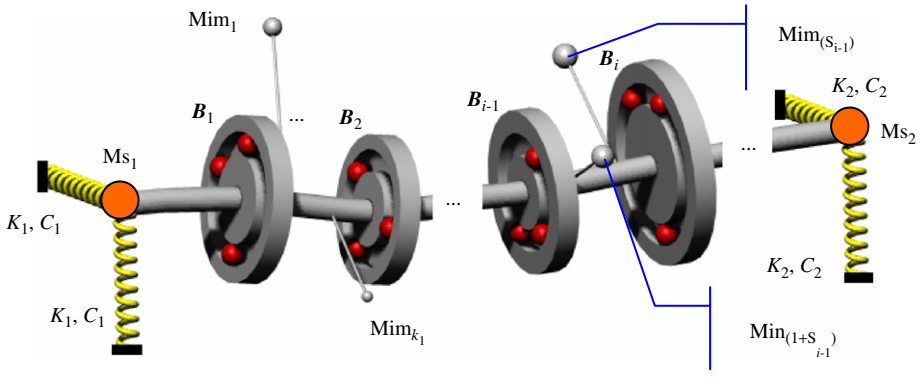

Fig. 1. A flexible rotor with discrete distributed unbalance masses, equipped with n ABB.

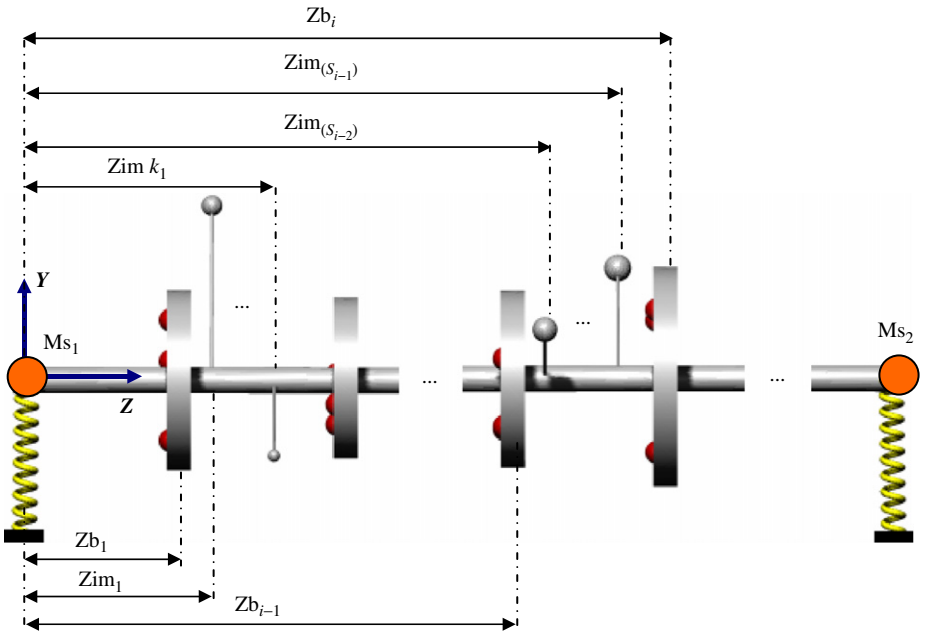

Fig. 2. The front view of the flexible shaft equipped with ABBs, and the positions of the ABBs and unbalanced masses.

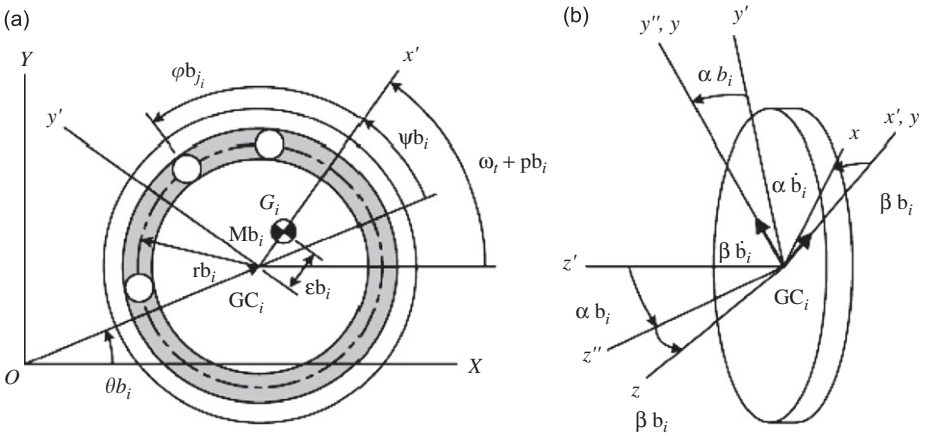

Fig. 3. Configuration of ith ABB in the Stodola–Green rotor model: (a) the configuration of the balancer after rotation of only ωt; (b) the configurations of the other Euler angles αb_i and βb_i [11].

reference frame and the points G_i and GC_i in Fig. 3 are the mass center and centroid of the ith rotor, respectively. The ABB consists of a circular rotor with a groove containing balls and a low viscosity damping fluid. The balls move freely in the groove and the rotor spins with an angular velocity of ω. Since the deflection of the shaft is generally small, it may be assumed that the centroid GC_i moves in the XY-plane. In Fig. 1, there are n ABBs, B_i is the index for the ith balancer. As shown in Fig. 1, there are k_1, k_2 and k_{i-1} number of point unbalanced masses, between balancer 1 and 2, balancer 2 and 3 and balancer $i-1$ and i, respectively. Also, $M\,\mathrm{im}_1$ and $M\,\mathrm{im}_{(S_{i-1})}$ are the masses of the first and the last unbalanced masses, respectively. C_1, K_1 and C_2, K_2 are the damping and stiffness coefficients of the first and second supports, respectively. Furthermore, Ms_1 and Ms_2 are the masses of the first and second supports, respectively.

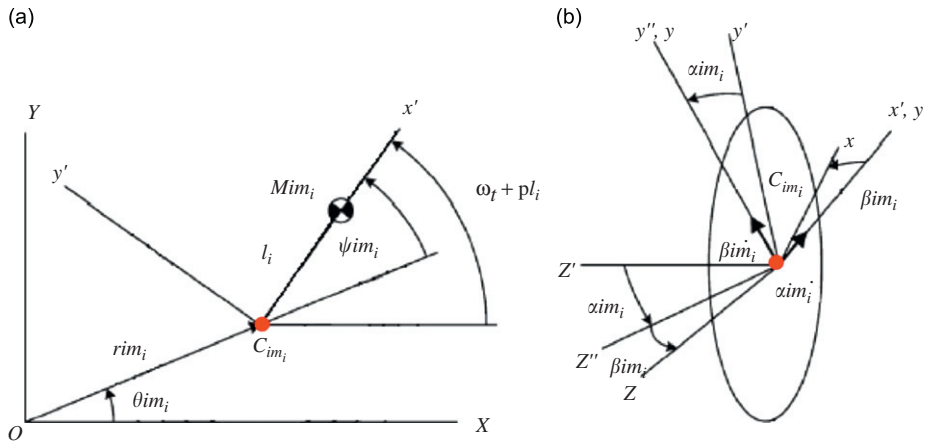

Fig. 4. Configuration of ith unbalanced mass in the Stodola–Green rotor model: (a) the configuration of the imbalance after rotation of only ωt; (b) the configurations of the other Euler angles $\alpha\,\mathrm{im}_i$, $\beta\,\mathrm{im}_i$.

In Fig. 2, Zb_i determines the position of the ith ABB from the left support. $Z\,\mathrm{im}_1$ and $Z\,\mathrm{im}_{k_1}$ are the positions of the first and the last unbalanced masses between ABB1 and 2, and $Z\,\mathrm{im}_{(1+S_{i-2})}$ and $Z\,\mathrm{im}_{(S_{i-1})}$ determine the positions of the first and the last unbalanced masses that lie between balancer $i-1$ and balancer i, from the left support. In the above figure, S_{i-1} and S_{i-2} are equal to $(k_1+k_2+\cdots+k_{i-1})$ and $(k_1+k_2+\cdots+k_{i-2})$, respectively.

To describe the rigid-body rotations of the rotor with respect to the X- or Y-axis, it is useful to consider the Euler angles which give the orientation of the rotor-fixed xyz coordinate system in comparison with the space-fixed XYZ coordinate system. In this study, the Euler angles $\omega t+pb_i$, αb_i and βb_i are used for orientations of ith ABB as shown in Fig. 3, pb_i is the initial angular position of the center of mass of the ith balancer relative to horizontal axis. In Fig. 3, Mb_i and εb_i are the mass and the eccentricity of the ith balancer, and rb_i and θb_i describe the radial and the angular positions of the geometric center of the ith balancer. The Euler angles $\omega t+pI_i$, $\alpha\,\mathrm{im}_i$ and $\beta\,\mathrm{im}_i$ are used for orientation of unbalanced-mass planes, as shown in Fig. 4. pI_i is the initial angular position of C_{im} (a point on the rotor axis, around which the ith unbalanced mass rotates) relative to horizontal axis. $M\,\mathrm{im}_i$ and l_i are the mass and the eccentricity of the ith unbalanced mass, and $r\,\mathrm{im}_i$ and $\theta\,\mathrm{im}_i$ describe the radial and the angular positions of C_{im_i}.

A rotation through an angle $\omega t+pb_i$ round the Z-axis results in the primed system, i.e., the $x'y'z'$ coordinate system. Rotation αb_i about the x'-axis puts the rotor into an orientation coincident to the double primed $x''y''z''$ coordinate system. Finally, a rotation of βb_i around the y''-axis yields the unprimed xyz coordinate system. These coordinate transformations can be arranged in the following matrix form:

$$\mathbf{x}'=\mathbf{T}_{\boldsymbol{\omega}}\mathbf{X},\quad \mathbf{x}''=\mathbf{T}_{\boldsymbol{\alpha b_i}}\mathbf{x}',\quad \mathbf{x}=\mathbf{T}_{\boldsymbol{\beta b_i}}\mathbf{x}'', \tag{1}$$

where

$$\mathbf{T}_{\boldsymbol{\omega}}=\begin{bmatrix}\cos(\omega t+pb_i) & \sin(\omega t+pb_i) & 0\\ -\sin(\omega t+pb_i) & \cos(\omega t+pb_i) & 0\\ 0 & 0 & 1\end{bmatrix},\quad \mathbf{T}_{\boldsymbol{\alpha b_i}}=\begin{bmatrix}1 & 0 & 0\\ 0 & \cos\alpha b_i & \sin\alpha b_i\\ 0 & -\sin\alpha b_i & \cos\alpha b_i\end{bmatrix}, \tag{2}$$

$$\mathbf{T}_{\boldsymbol{\beta b_i}}=\begin{bmatrix}\cos\beta b_i & 0 & -\sin\beta b_i\\ 0 & 1 & 0\\ \sin\beta b_i & 0 & \cos\beta b_i\end{bmatrix}$$

$$\mathbf{X}=X\hat{\mathbf{I}}+Y\hat{\mathbf{J}}+Z\hat{\mathbf{K}},\quad \mathbf{x}'=x'\mathbf{i}'+y'\mathbf{j}'+z'\mathbf{k}',\quad \mathbf{x}''=x''\mathbf{i}''+y''\mathbf{j}''+z''\mathbf{k}'',\quad \mathbf{x}=x\mathbf{i}+y\mathbf{j}+z\mathbf{k} \tag{3}$$

in which $\hat{\mathbf{I}},\hat{\mathbf{J}}$ and $\hat{\mathbf{K}}$ are the unit vectors along the X-, Y- and Z-axis; $\mathbf{i}',\mathbf{j}'$ and $\mathbf{k}'$ are the unit vectors along the x'-, y'- and z'-axis; $\mathbf{i}$, $\mathbf{j}$ and $\mathbf{k}$ are the unit vectors along the x-, y- and z-axis, respectively.

First, consider the kinetic energy of the rotor system with the ABBs. The position vector of the mass center G_i of the ith ABB can be expressed in the xyz coordinate system by using the rotation matrices, $\mathbf{T}_{\omega}$, $\mathbf{T}_{\alpha \mathbf{b}_i}and\mathbf{T}_{\beta \mathbf{b}_i}$:

$$\mathbf{rgb}_i = \mathbf{T}_{\beta \mathbf{b}_i}\mathbf{T}_{\alpha \mathbf{b}_i}\mathbf{T}_{\omega}\mathbf{r}_{O_iC_i/XYZ} + \mathbf{r}_{C_iG_i}, \tag{4}$$

where

$$\mathbf{r}_{O_iC_i/XYZ} = \mathbf{rb}_i(\cos\,\theta b_i\hat{\mathbf{I}} + \sin\,\theta b_i\hat{\mathbf{J}}), \quad \mathbf{r}_{C_iG_i} = \varepsilon b_i\mathbf{i}. \tag{5}$$

We use a new generalized coordinate $\psi \mathrm{b}_i$ defined by

$$\psi b_i = \omega t + pb_i - \theta b_i. \tag{6}$$

The position vector of the mass center of the ith balancer, $\mathbf{rgb}_i$, and the position vector of the jth ball of the ith ABB B_{ij}, $\mathbf{rb}_{ij}$, can be written as

$$\begin{aligned}\mathbf{rgb}_i = {} & (rb_i(\cos(\beta b_i)\,\cos(\psi b_i) - \sin(\alpha b_i)\,\sin(\beta b_i)\,\sin(\psi b_i)) + \varepsilon b_i)\mathbf{i} \\ & - rb_i\cos(\alpha b_i)\,\sin(\psi b_i)\mathbf{j} + (rb_i(\sin(\beta b_i)\,\cos(\psi b_i) \\ & + \sin(\alpha b_i)\,\cos(\beta b_i)\,\sin(\psi b_i)))\mathbf{k}\end{aligned} \tag{7}$$

$$\begin{aligned}\mathbf{rb}_{ij} = {} & [rb_i(\cos(\beta b_i)\,\cos(\psi b_i) - \sin(\alpha b_i)\,\sin(\beta b_i)\,\sin(\psi b_i)) + r_i\,\cos\,\varphi b_{ij}]\mathbf{i} \\ & + (-rb_i\,\cos(\alpha b_i)\,\sin(\psi b_i) + r_i\,\sin\,\varphi b_{ij})\mathbf{j} \\ & + rb_i(\sin(\beta b_i)\,\cos(\psi b_i) + \sin(\alpha b_i)\,\cos(\beta b_i)\,\sin(\psi b_i))\mathbf{k}\end{aligned} \tag{8}$$

When the system has n ABBs with p balls in each ABB, the kinetic energy T_1 is given by

$$T_1 = \sum_{i=1}^{n}\left(\frac{1}{2}\boldsymbol{\omega}\mathbf{b}_i^{\mathrm{T}}\mathbf{Jb}_i\boldsymbol{\omega}\mathbf{b}_i + \frac{1}{2}Mb_i\frac{\mathrm{d}(\mathbf{rgb}_i)}{\mathrm{d}t}\frac{\mathrm{d}(\mathbf{rgb}_i)}{\mathrm{d}t}\right) + \frac{1}{2}m\sum_{i=1}^{n}\sum_{j=1}^{p}\frac{\mathrm{d}(\mathbf{rb}_{ij})}{\mathrm{d}t}\frac{\mathrm{d}(\mathbf{rb}_{ij})}{\mathrm{d}t} \tag{9}$$

where $\mathbf{Jb}_i$ is the inertia matrix of ith ball-balancer and $\boldsymbol{\omega}\mathbf{b}_i$ is the angular velocity of ith ball-balancer.

$$\mathbf{Jb}_i = \begin{bmatrix} Jb_i & 0 & 0 \\ 0 & Jb_i & 0 \\ 0 & 0 & JZb_i \end{bmatrix} \tag{10}$$

$$\boldsymbol{\omega}\mathbf{b}_i = (-\omega\,\cos\,\alpha b_i + \alpha\dot{b}_i\,\cos\,\beta b_i)\mathbf{i} + (\omega\,\sin\,\alpha b_i + \beta\dot{b}_i)\mathbf{j} + (\omega\,\cos\,\alpha b_i\,\cos\,\beta b_i + \alpha\dot{b}_i\,\sin\,\beta b_i)\mathbf{k} \tag{11}$$

in which Jb_i is the mass moment of inertia about the x- or y-axis and JZb_i is the mass moment of inertia about the z-axis. Using the same method described above the position of ith unbalanced mass is obtained as below:

$$\begin{aligned}\mathbf{rimb}_i = {} & (r\,\mathrm{im}_i(\cos(\beta\,\mathrm{im}_i).\cos(\psi\,\mathrm{im}_i) - \sin(\alpha\,\mathrm{im}_i).\sin(\beta\,\mathrm{im}_i).\sin(\psi\,\mathrm{im}_i)) + l_i)\mathbf{i} \\ & - r\,\mathrm{im}_i\cos(\alpha\,\mathrm{im}_i).\sin(\psi\,\mathrm{im}_i)\mathbf{j} + (r\,\mathrm{im}_i(\sin(\beta\,\mathrm{im}_i).\cos(\psi\,\mathrm{im}_i) \\ & + \sin(\alpha\,\mathrm{im}_i).\cos(\beta\,\mathrm{im}_i).\sin(\psi\,\mathrm{im}_i)))\mathbf{k}\end{aligned} \tag{12}$$

where

$$\psi\,\mathrm{im}_i = \omega t + pI_i - \theta\,\mathrm{im}_i. \tag{13}$$

The kinetic energy due to the unbalanced masses and mass of the supports is calculated simply as

$$T_2 = \frac{1}{2}\sum_{i=1}^{q}M\,\mathrm{im}_i\frac{\mathrm{d}(\mathbf{rim}\,\mathbf{b}_i)}{\mathrm{d}t}\frac{\mathrm{d}(\mathbf{rim}\,\mathbf{b}_i)}{\mathrm{d}t} + \frac{1}{2}\sum_{i=1}^{2}\mathrm{Ms}_i\frac{\mathrm{d}(\mathbf{rs}_i)}{\mathrm{d}t}\frac{\mathrm{d}(\mathbf{rs}_i)}{\mathrm{d}t} \tag{14}$$

In the above equation, rs_i ($i = 1,2$) shows the radial position of the supports. Finally, the kinetic energy of the system is obtained by adding Eqs. (9) and (14).

$$T = T_1 + T_2 \tag{15}$$

Neglecting the gravity and the torsional and longitudinal deflections of the shaft [11], the potential energy, or the strain energy, is obtained from the bending deflection of the shaft. As shown in Fig. 1 the shaft has two elastic supports, and unbalanced masses are distributed along the shaft. It is clear that the deflection curves vary in different parts as shown in Fig. 2. For simplicity, we define a general deflection curve based on the strength of material science and then satisfy the boundary conditions. Since one end of part 1 is on the left support and the bending moment is zero at this point, the general deflection curve in the x-direction for this part is

$$\delta x_1 = A1.Z^3 + A2.Z + A3 \tag{16}$$

where $A1$, $A2$ and $A3$ are parameters obtained from the boundary conditions as below:

$$\text{at } Z = 0 \quad \{\delta x_1 = dsx_1$$

$$\text{at } Z = zb_1 \quad \begin{cases} \delta x_1 = dbx_1 \\ \mathrm{d}/\mathrm{d}Z(\delta x_1) = pby_1 \end{cases} \tag{17}$$

In the above equations, pby_1, dsx_1 and dbx_1 are slope at $Z = Zb_1$ and the deflections at $Z = 0$ and $Z = Zb_1$ in the ZX-plane, respectively. Similarly, the deflection curve in the y-direction for this part is

$$\delta y_1 = A1{*}Z^3 + A2{*}Z + A3 \tag{18}$$

where

$$\text{at } Z = 0 \quad \{\delta y_1 = dsy_1$$

$$\text{at } Z = zb_1 \quad \begin{cases} \delta y_1 = dby_1 \\ \mathrm{d}/\mathrm{d}Z(\delta y_1) = -pbx_1 \end{cases} \tag{19}$$

pbx_1, dsy_1 and dby_1 are slope at $Z = Zb_1$ and the deflections at $Z = 0$ and $Z = Zb_1$ in the ZY-plane, respectively. The same relations mentioned above can be obtained for the last part as follows:

$$\delta x_{n+q+1} = A1{*}(Z - L)^3 + A2{*}(Z - L) + A3 \tag{20}$$

where

$$\text{at } Z = zb_n \quad \begin{cases} \delta x_{n+q+1} = dbx_n \\ \mathrm{d}/\mathrm{d}Z(\delta x_{n+q+1}) = pby_n \end{cases}$$

$$\text{at } Z = L \quad \{\delta x_{n+q+1} = dsx_2 \tag{21}$$

and

$$\delta y_{n+q+1} = A1{*}(Z - L)^3 + A2{*}(Z - L) + A3 \tag{22}$$

where

$$\text{at } Z = zb_n \quad \begin{cases} \delta y_{n+q+1} = dby_n \\ \mathrm{d}/\mathrm{d}Z(\delta y_{n+q+1}) = -pbx_n \end{cases} \tag{23}$$

$$\text{at } Z = L \quad \{\delta y_{n+q+1} = dsy_2$$

For other parts shown in Fig. 2, the general deflection curve in the ZX- and ZY-plane is

$$\delta x, y_i = A1.Z^3 + A2.Z^2 + A3.Z + A4, \quad 2 \leqslant i \leqslant n + q \tag{24}$$

where $A1$, $A2$, $A3$ and $A4$ are the parameters defined from boundary conditions and index i indicates the number of parts. In the relations described above for the deflection curve of the shaft, geometric relations between parameters are as follows:

$$dsx_i = rs_i \cos(\theta s_i), \quad i = 1, 2$$

$$dsy_i = rs_i \sin(\theta s_i), \quad i = 1,2 \tag{25}$$

$$dbx_i = rb_i \cos(\theta b_i), \quad i = 1,\ldots,n$$

$$dby_i = rb_i \sin(\theta b_i), \quad i = 1,\ldots,n$$

$$pby_i = \alpha b_i \sin(\omega t + pb_i) + \beta b_i \cos(\alpha b_i)\cos(\omega t + pb_i), \quad i = 1,\ldots,n$$

$$pbx_i = \alpha b_i \cos(\omega t + pb_i) - \beta b_i \cos(\alpha b_i)\sin(\omega t + pb_i), \quad i = 1,\ldots,n \tag{26}$$

$$d\,\mathrm{im}\,x_i = r\,\mathrm{im}_i \cos(\theta\,\mathrm{im}_i), \quad i = 1,\ldots,q$$

$$d\,\mathrm{im}\,y_i = r\,\mathrm{im}_i \sin(\theta\,\mathrm{im}_i), \quad i = 1,\ldots,q$$

$$p\,\mathrm{im}y_i = \alpha\,\mathrm{im}_i \sin(\omega t + pI_i) + \beta\,\mathrm{im}_i \cos(\alpha\,\mathrm{im}_i)\cos(\omega t + pI_i), \quad i = 1,\ldots,q$$

$$p\,\mathrm{im}x_i = \alpha\,\mathrm{im}_i \cos(\omega t + pI_i) - \beta\,\mathrm{im}_i \cos(\alpha\,\mathrm{im}_i)\sin(\omega t + pI_i), \quad i = 1,\ldots,q \tag{27}$$

In the above, dsx_i and dsy_i are the deflections of the shaft at the ith support in the x and y directions, respectively. In relation (25), θs_i ($i = 1,2$) shows the angular position of supports. Also, dbx_i and dby_i are the deflections of the shaft at the centroid of the ith ABB in the x and y directions, respectively. Furthermore, pbx_i and pby_i are the slopes at the centroid of the ith ABB, in the zy- and zx-planes, respectively. The deflection and slope of the point on the shaft that determine the position of ith unbalance mass, C_{im}, in the ZX- and ZY-planes are as relations (27). n and q are the number of ABBs and unbalanced masses, respectively. Finally, after defining these coefficients i.e., $A1$, $A2$, $A3$ and $A4$ for each part, we can obtain the strain energy of the system as below:

$$V_1 = \frac{1}{2}EI\left[\begin{array}{c}
\displaystyle\sum_{q=2}^{n}\sum_{i=\sum_{j=1}^{q-1}k_{j-1}+2}^{\sum_{j=1}^{q-1}k_j}\int_{Z\,\mathrm{im}_{i-1}}^{Z\,\mathrm{im}_i}\left[\left(\frac{\partial^2(\delta x_{i+q-1})}{\partial Z^2}\right)^2+\left(\frac{\partial^2(\delta y_{i+q-1})}{\partial Z^2}\right)^2\right]\mathrm{d}Z \\
+\displaystyle\sum_{i=2}^{n}\left(\int_{Zb_{i-1}}^{Z\,\mathrm{im}_{S_{i-2}+1}}\left[\left(\frac{\partial^2(\delta x_{S_{i-2}+i})}{\partial Z^2}\right)^2+\left(\frac{\partial^2(\delta x_{S_{i-2}+i})}{\partial Z^2}\right)^2\right]\mathrm{d}Z\right) \\
+\displaystyle\sum_{i=2}^{n}\left(\int_{Z\,\mathrm{im}_{S_{i-1}}}^{Zb_i}\left[\left(\frac{\partial^2(\delta x_{S_{i-1}+i})}{\partial Z^2}\right)^2+\left(\frac{\partial^2(\delta x_{S_{i-1}+i})}{\partial Z^2}\right)^2\right]\mathrm{d}Z\right) \\
+\displaystyle\int_0^{Zb_1}\left(\left(\frac{\partial^2(\delta x_1)}{\partial Z^2}\right)^2+\left(\frac{\partial^2(\delta y_1)}{\partial Z^2}\right)^2\right)\mathrm{d}Z+\int_{Zb_n}^{L}\left(\left(\frac{\partial^2(\delta x_{S_{n-1}+1})}{\partial Z^2}\right)^2+\left(\frac{\partial^2(\delta y_{S_{n-1}+1})}{\partial Z^2}\right)^2\right)\mathrm{d}Z
\end{array}\right]$$

where

$$S_{i-1} = k_1 + k_2 + \cdots + k_{i-1},$$

$$S_{i-2} = k_1 + k_2 + \cdots + k_{i-2},$$

$$S_{n-1} = k_1 + k_2 + \cdots + k_{n-1}. \tag{28}$$

In the above, E is Young's modulus and I is the area moment of inertia of the shaft cross-section.

The potential energy of the system due to the linear springs in the supports is

$$V_2 = \tfrac{1}{2}(K_1(dsx_1^2 + dsy_1^2) + K_2(dsx_2^2 + dsy_2^2)) \tag{29}$$

The total potential energy of the system is

$$V = V_1 + V_2 \tag{30}$$

Furthermore, Rayleigh's dissipation function, F, can be represented by

$$F = \frac{1}{2}\sum_{i=1}^{n}(ct_i(r\dot{b}_i^2 + rb_i^2\cdot\theta\dot{b}_i^2) + cr_i(\alpha\dot{b}_i^2 + \beta\dot{b}_i^2)) + \frac{1}{2}\sum_{i=1}^{2} C_i(r\dot{s}_i^2 + rs_i^2\theta\dot{s}_i^2) + \frac{1}{2}\sum_{i=1}^{n}\sum_{j=1}^{p} D_i\cdot p\dot{b}_{ij}^2 \tag{31}$$

where ct_i is the equivalent damping coefficient for translation of the ith ABB, cr_i is the equivalent damping coefficient of rotation of ith ABB, and D_i is the viscous drag coefficient of the ball in the damping fluid of the ith ABB. It is assumed that the balls in each balancer have the same viscous drag coefficient of D_i.

The equations of motion for the system are derived by Lagrange's equation given by

$$\frac{\mathrm{d}}{\mathrm{d}t}\left(\frac{\partial T}{\partial\dot{q}_k}\right) - \frac{\partial T}{\partial q_k} + \frac{\partial V}{\partial q_k} + \frac{\partial F}{\partial\dot{q}_k} = 0 \tag{32}$$

where q_k is the generalized coordinate. For the given system, the generalized coordinates are

$$\{rs_i, \psi s_i i = 1,2\}, \quad \{rb_i, \psi b_i, \alpha b_i, \beta b_i, \varphi b_{ij} \quad i = 1,2,\ldots,n, \ \ j = 1,2,\ldots,p\},$$

$$\{r\,\mathrm{im}_i, \psi\,\mathrm{im}_i, \alpha\,\mathrm{im}_i, \beta\,\mathrm{im}_i \quad i = 1,2,\ldots,q\} \tag{33}$$

Therefore, the dynamic behavior of the balancer is governed by $4(n+q)+np+4$ independent equations of motion. Substituting Eqs. (15), (30) and (31) into Eq. (32) yields the equations of motion. The derived equations are so long and complex that they cannot be represented in this paper. The whole process of the derivation of the equations of motion is computerized using Matlab and Maple softwares, and the derived equations are saved as text files. The information of these text files are used for extracting the equilibrium positions and linearized equations of motion.

3. Equilibrium positions and linearized equations

The equations of motion derived in the previous section can be described as below:

$$\mathbf{G}(\mathbf{x},\dot{\mathbf{x}},\ddot{\mathbf{x}}) = \mathbf{M}(\mathbf{x})\ddot{\mathbf{x}} + \mathbf{N}(\mathbf{x},\dot{\mathbf{x}}) = 0 \tag{34}$$

where $\mathbf{M}$ is the mass matrix, $\mathbf{N}$ is the nonlinear internal force vector, and $\mathbf{x}$ is the displacement vector:

$$\mathbf{x} = \{rs_i, \psi s_i, rb_j, \psi b_j, \alpha b_j, \beta b_j, \varphi_{jl}, r\,\mathrm{im}_t, \psi\,\mathrm{im}_t, \alpha\,\mathrm{im}_t, \beta\,\mathrm{im}_t\}^{\mathrm{T}}$$

$$\begin{cases} i = 1,2 \\ j = 1,2,\ldots,n \quad (n = \text{number of auto ball-balancers}) \\ l = 1,2,\ldots,p \quad (p = \text{number of balls in each auto ball-balancers}) \\ t = 1,2,\ldots,q \quad (q = \text{number of unbalance masses}) \end{cases} \tag{35}$$

The stability analysis for a non-autonomous system is very cumbersome and a time consuming process. By substituting the relations below into the derived equations of motion, the equations of motion for an autonomous system can be achieved.

$$\psi s_i = \omega t - \theta s_i, \quad i = 1,2$$

$$\psi b_i = \omega t - \theta b_i, \quad i = 1,2,\ldots,n$$

$$\psi\,\mathrm{im}_i = \omega t - \theta\,\mathrm{im}_i, \quad i = 1,2,\ldots,q \tag{36}$$

The state equations can be used clearly for stability analysis, utilizing the notations:

$$\left\{\begin{array}{ccccc} \dot{r}s_i = r\hat{s}_i, & \dot{\psi}s_i = \psi\hat{s}_i, & & & \\ \dot{r}b_j = r\hat{b}_j, & \dot{\psi}b_j = \psi\hat{b}_j, & \dot{\alpha}b_j = \alpha\hat{b}_j, & \dot{\beta}b_j = \beta\hat{b}_j, & \dot{\varphi}_{jl} = \hat{\varphi}_{jl}, \\ r\,\dot{\mathrm{im}}_t = r\,\hat{\mathrm{im}}_t, & \dot{\psi}\,\mathrm{im}_t = \hat{\psi}\,\mathrm{im}_t, & \alpha\,\dot{\mathrm{im}}_t = \alpha\,\hat{\mathrm{im}}_t, & \beta\,\dot{\mathrm{im}}_t = \beta\,\hat{\mathrm{im}}_t, & \end{array}\right\}$$

where

$$\begin{cases} i = 1,2 \\ j = 1,2,\ldots,n \quad (n = \text{number of ball-balancers}) \\ l = 1,2,\ldots,p \quad (p = \text{number of balls in each balancer}) \\ t = 1,2,\ldots,q \quad (q = \text{number of unbalance masses}) \end{cases} \tag{37}$$

The equations of motion can be expressed as follows:

$$\mathbf{A}(\mathbf{x})\dot{\mathbf{x}} = \mathbf{N}(\mathbf{x}) \tag{38}$$

where

$$\mathbf{x} = \left\{ \begin{array}{l} rs_i, \psi s_i, rb_j, \psi b_j, \alpha b_j, \beta b_j, \varphi_{jl}, r\,\mathrm{im}_t, \psi\,\mathrm{im}_t, \alpha\,\mathrm{im}_t, \beta\,\mathrm{im}_t, \\ \hat{r}s_i, \hat{\psi}s_i, \hat{r}b_j, \hat{\psi}b_j, \hat{\alpha}b_j, \hat{\beta}b_j, \hat{\varphi}_{jl}, r\,\hat{\mathrm{im}}_t, \hat{\psi}\,\mathrm{im}_t, \alpha\,\hat{\mathrm{im}}_t, \beta\,\hat{\mathrm{im}}_t \end{array} \right\}^{\mathrm{T}} \tag{39}$$

The indexes i, j, l and t are determined from the relation (37). The perturbation method is used to obtain linearized equations of motion in the neighborhood of the equilibrium positions. The generalized coordinates (33) can be represented by

$$rs_i = rs_i^* + \Delta rs_i, \quad \psi s_i = \psi s_i^* + \Delta\psi s_i, \quad i = 1,2$$

$$rb_i = rb_i^* + \Delta rb_i, \quad \psi b_i = \psi b_i^* + \Delta\psi b_i, \quad \alpha b_i = \alpha b_i^* + \Delta\alpha b_i, \quad \beta b_i = \beta b_i^* + \Delta\beta b_i, \quad \varphi_{ij} = \varphi_{ij}^* + \Delta\varphi_{ij}$$
$$(i = 1,2,\ldots n \quad \text{and} \quad j = 1,2,\ldots,p)$$

$$r\,\mathrm{im}_i = r\,\mathrm{im}_i^* + \Delta r\,\mathrm{im}_i, \quad \psi\,\mathrm{im}_i = \psi\,\mathrm{im}_i^* + \Delta\psi\,\mathrm{im}_i, \quad \alpha\,\mathrm{im}_i = \alpha\,\mathrm{im}_i^* + \Delta\alpha\,\mathrm{im}_i, \quad \beta\,\mathrm{im}_i = \beta\,\mathrm{im}_i^* + \Delta\beta\,\mathrm{im}_i$$
$$(i = 1,2,\ldots,q) \tag{40}$$

For simplicity the relations (40) can be rewritten as below:

$$\mathbf{x} = \mathbf{x}^* + \Delta\mathbf{x} \tag{41}$$

where the starred parameters are the coordinates of an equilibrium position and the parameters with Δ are the small perturbations of the generalized coordinates in the neighborhood of the equilibrium position. Generally, the equilibrium positions may be classified into two cases: balanced and unbalanced. In the first case, it is respected that all the radial displacements and angle deviations converge to zero and angular position of the balls are definite quantities. In the second case all the quantities are non-zero. It is clear that ideal results are obtained in the first case, but in the system of an unbalanced rotating shaft equipped with n ball-balancer, the balanced equilibrium position does not exist. In order to determine the positions for the unbalanced case, it needs to substitute the relation (42) into the equations of motion in the state space (38).

$$\dot{\mathbf{x}} = 0 \tag{42}$$

This substitution leads to a set of nonlinear equations, i.e., $\mathbf{N}(\mathbf{x}^*) = 0$, where $\mathbf{x}^*$ shows the equilibrium positions. Obviously these set of equations do not have any closed form solution and only the numerical methods must be employed. So, the equilibrium positions cannot be defined parametric. Matlab software is a suitable solution for this problem. Authors wrote a program whose output is the equilibrium positions.

In order to obtain the linear variational equations of motion, Eq. (38) is linearized in the neighborhood of the equilibrium positions. Substituting Eq. (41) into Eq. (38) yields the following:

$$\mathbf{A}(\mathbf{x}^* + \Delta\mathbf{x})\Delta\dot{\mathbf{x}} = \mathbf{N}(\mathbf{x}^* + \Delta\mathbf{x}) \tag{43}$$

which may be rewritten as below:

$$\mathbf{A}(\mathbf{x}^* + \Delta\mathbf{x})\Delta\dot{\mathbf{x}} = N(\mathbf{x}^* + \Delta\mathbf{x}) - \mathbf{N}(\mathbf{x}^*) \tag{44}$$

Expanding the above equation about $\Delta\mathbf{x} = 0$, the following equation is achieved:

$$\mathbf{A}^*\Delta\dot{\mathbf{x}} = \mathbf{B}^*\Delta\mathbf{x} + \mathbf{O}(\Delta\mathbf{x}) \tag{45}$$

In the above equation $\mathbf{A}^*$ and $\mathbf{B}^*$ are constant and $\mathbf{O}$ is a function of the second order of $\Delta\mathbf{x}$ or higher. If $\Delta\mathbf{x}$ is sufficiently small, then $\mathbf{O}(\Delta\mathbf{x})$ can be neglected and as such, the linearized equations of motion about the

equilibrium positions are obtained as below:

$$\mathbf{A}^*\Delta\dot{\mathbf{x}} = \mathbf{B}^*\Delta\mathbf{x} \tag{46}$$

where

$$\mathbf{A}^* = \begin{bmatrix} \mathbf{I} & 0 \\ 0 & \mathbf{M} \end{bmatrix}, \quad \mathbf{B}^* = \begin{bmatrix} 0 & \mathbf{I} \\ \mathbf{K}^* & \mathbf{C}^* \end{bmatrix} \tag{47}$$

$\mathbf{I}$, $\mathbf{M}$ are identity and mass matrices of order $4(n+q)+np+4$, respectively.

$\mathbf{K}^*$ and $\mathbf{C}^*$ in relation (47) are as follows:

$$\mathbf{K}^* = \begin{bmatrix} -\dfrac{\partial F_1}{\partial X_1} & -\dfrac{\partial F_1}{\partial X_2} & \cdots & -\dfrac{\partial F_1}{\partial X_{4(n+q)+np+4}} \\ -\dfrac{\partial F_2}{\partial X_1} & -\dfrac{\partial F_2}{\partial X_2} & \cdots & -\dfrac{\partial F_2}{\partial X_{4(n+q)+np+4}} \\ \vdots & \vdots & \vdots & \vdots \\ -\dfrac{\partial F_{4(n+q)+np+4}}{\partial X_1} & -\dfrac{\partial F_{4(n+q)+np+4}}{\partial X_2} & \cdots & -\dfrac{\partial F_{4(n+q)+np+4}}{\partial X_{4(n+q)+np+4}} \end{bmatrix} \tag{48}$$

$$\mathbf{C}^* = \begin{bmatrix} -\dfrac{\partial F_1}{\partial Y_1} & -\dfrac{\partial F_1}{\partial Y_2} & \cdots & -\dfrac{\partial F_1}{\partial Y_{4(n+q)+np+4}} \\ -\dfrac{\partial F_2}{\partial Y_1} & -\dfrac{\partial F_2}{\partial Y_2} & \cdots & -\dfrac{\partial F_2}{\partial Y_{4(n+q)+np+4}} \\ \vdots & \vdots & \vdots & \vdots \\ -\dfrac{\partial F_{4(n+q)+np+4}}{\partial Y_1} & -\dfrac{\partial F_{4(n+q)+np+4}}{\partial Y_2} & \cdots & -\dfrac{\partial F_{4(n+q)+np+4}}{\partial Y_{4(n+q)+np+4}} \end{bmatrix} \tag{49}$$

In the above couple of matrices, $F_1, F_2, \ldots, F_{4(n+q)+np+4}$ are the $4(n+q)+np+4$ equations which are obtained from $\mathbf{N}(\mathbf{x}^*)=0$. Also, $X_1, X_2, \ldots, X_{4(n+q)+np+4}$ and $Y_1, Y_2, \ldots, Y_{4(n+q)+np+4}$ are the first and second $4(n+q)+np+4$ elements of vector $\mathbf{x}$ in relation (39).

It must be noted that Eq. (46) is valid only in the neighborhood of the equilibrium positions.

4. Stability analysis

The stability of the system is analyzed with linearized equations of motion in the neighborhood of the equilibrium position. For simplicity, it is assumed that the number of ball-balancers and unbalanced masses are 1 and 2, respectively, i.e., $n=2$ and $q=1$. Also, there are two balls in the groove of each ball-balancer. The mass moments of inertia Jb_i and JZb_i are given by

$$Jb_i = \tfrac{1}{4}Mb_iR_i^2, \quad JZb_i = \tfrac{1}{2}Mb_iR_i^2 \tag{50}$$

Mb_i and R_i are the mass and radius of the ith ball-balancer.

Stability analysis can be investigated utilizing the characteristic value problem for Eq. (46).

Small perturbations of the generalized coordinates from the equilibrium position can be written as

$$\Delta rs_i = X_{rs_i}e^{\lambda t}, \quad \Delta\psi s_i = X_{\psi s_i}e^{\lambda t}, \quad \Delta rb_j = X_{rb_j}e^{\lambda t}, \quad \Delta\psi b_j = X_{\psi b_j}e^{\lambda t},$$

$$\Delta\alpha b_j = X_{\alpha b_j}e^{\lambda t}, \quad \Delta\beta b_j = X_{\beta b_j}e^{\lambda t}, \quad \Delta\varphi_{jl} = X_{\varphi_{jl}}e^{\lambda t}, \quad \Delta r\,\mathrm{im}_t = X_{r\,\mathrm{im}_t}e^{\lambda t},$$

$$\Delta\psi\,\mathrm{im}_t = X_{\psi\,\mathrm{im}_t}e^{\lambda t}, \quad \Delta\alpha\,\mathrm{im}_t = X_{\alpha\,\mathrm{im}_t}e^{\lambda t}, \quad \Delta\beta\,\mathrm{im}_t = X_{\beta\,\mathrm{im}_t}e^{\lambda t} \tag{51}$$

Table 1
System parameters.

Parameters	Value	Description
E	207 GPa	Elasticity modules
r_{Shaft}	20 mm	The radius of the shaft
L	2 m	The length of the shaft
ω	300 rad s^{-1}	Angular velocity of the shaft
Ms_1, Ms_2	1 kg	The mass of the supports
$Mb_1 = Mb_2$	12 kg	The mass of the auto ball-balancers
$R_1 = R_2$	0.12 m	The radius of the auto ball-balancers
zb_1	$L/4$ m	The position of the first auto ball-balancer relative to fixed coordinate system
zb_2	$3L/4$ m	The position of the second auto ball-balancer relative to fixed coordinate system
$\varepsilon b_1 = \varepsilon b_2$	0.000001 m	Eccentricity of the auto ball-balancers
$D_1 = D_2$	3.6 N m s^2	Viscous damping coefficient
$mb_{11} = mb_{12} = mb_{21} = mb_{22}$	510 g	The mass of freely moving balls
$z\,\mathrm{im}_1$	L/2 m	The position of unbalanced mass relative to fixed coordinate system
l_1	0.1 m	Vertical distance of unbalanced mass from axis of the shaft
$m\,\mathrm{im}_1$	1.9 kg	Mass of unbalancing
$C_1 = C_2$	0.03 N m s^{-1}	Damping coefficient of supports
$K_1 = K_2$	50 N mm^{-1}	Stiffness coefficient of supports

where,

$$i,j,l = 1,2 \quad \text{and} \quad t = 1 \tag{52}$$

Substituting the above into the linearized equations of motion leads to the following equation:

$$|\mathbf{B}^* - \lambda \mathbf{A}^*| = 0 \tag{53}$$

This is the condition that equations in (46) have non-trivial solutions and can be expressed as the characteristics equation as below:

$$\sum_{k=0}^{40} c_k \lambda^k = 0 \tag{54}$$

where the coefficients c_k $(k = 0, 1, \ldots, 40)$ are functions of the system parameters, such as $\omega, r_{Shaft}, L, C_1, C_2, K_1, K_2$ and …. Since the coefficients c_k are complicated functions of the system parameters, the explicit expressions are omitted from this paper.

The Routh–Hurwitz criteria are used to investigate stability of the system of auto ball-balancers. If all the eigenvalues, namely, the roots of Eq. (54), have negative real parts, the system of ball-balancers is asymptotically stable. The Routh–Hurwitz criteria provide the necessary and sufficient conditions for the real parts of all roots to be negative. The parameters in Table 1 are used for stability analysis and calculating the natural frequencies of the system.

Denoting the natural frequencies of the system without balls by $\omega_1, \omega_2, \ldots, \omega_8$, these natural frequencies can be obtained from

$$\begin{bmatrix} ms_1 & 0 & 0 & 0 & 0 & 0 & 0 & 0 \\ 0 & Mb_1 & 0 & 0 & 0 & 0 & 0 & 0 \\ 0 & 0 & J_1 & 0 & 0 & 0 & 0 & 0 \\ 0 & 0 & 0 & m\,\mathrm{im}_1 & 0 & 0 & 0 & 0 \\ 0 & 0 & 0 & 0 & J_{\mathrm{im}} & 0 & 0 & 0 \\ 0 & 0 & 0 & 0 & 0 & Mb_2 & 0 & 0 \\ 0 & 0 & 0 & 0 & 0 & 0 & J_2 & 0 \\ 0 & 0 & 0 & 0 & 0 & 0 & 0 & Ms_2 \end{bmatrix} \begin{Bmatrix} r\ddot{s}_1 \\ r\ddot{b}_1 \\ \alpha\ddot{b}_1 \\ r\,\mathrm{i}\ddot{m}_1 \\ \alpha\,\mathrm{i}\ddot{m}_1 \\ r\ddot{b}_2 \\ \alpha\ddot{b}_2 \\ r\ddot{s}_2 \end{Bmatrix}$$

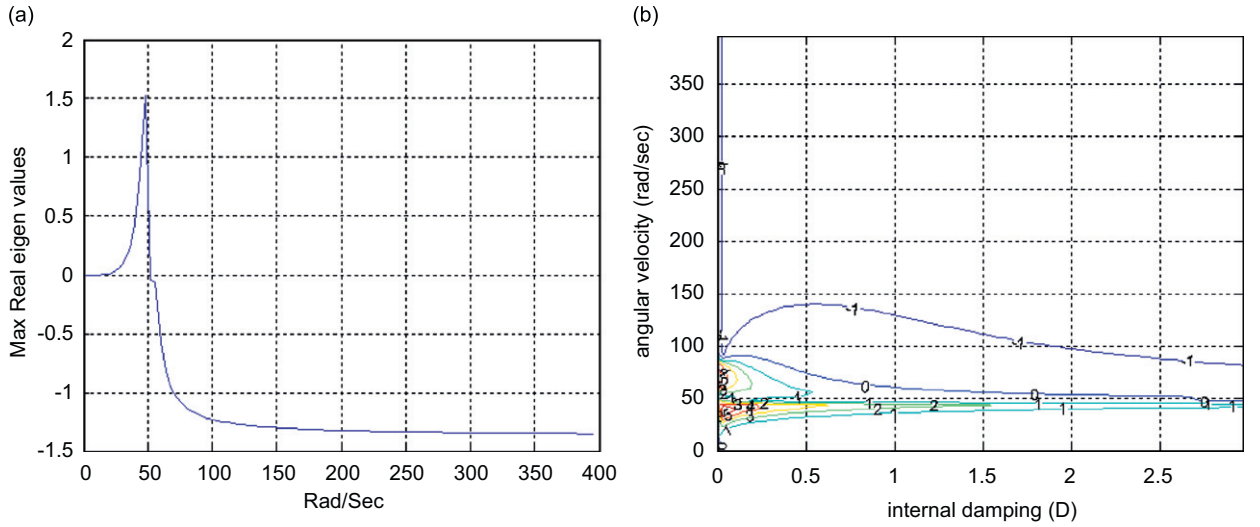

Fig. 5. Balanced stable region: (a) variation of angular velocity in terms of the max. Real eigenvalues of the characteristic equation, (b) variation of the internal damping (fluid damping) in terms of the angular velocity.

$$+\frac{8EI}{L^3}\begin{bmatrix} 24+\frac{K_1L^3}{EI} & -24 & 6L & 0 & 0 & 0 & 0 & 0 \\ -24 & 120 & 6L & -96 & 12L & 0 & 0 & 0 \\ 6L & 6L & \frac{7L^2}{2} & -12L & L^2 & 0 & 0 & 0 \\ 0 & -96 & -12L & 192 & 0 & -96 & 12L & 0 \\ 0 & 12L & L^2 & 0 & 4L^2 & -12L & L^2 & 0 \\ 0 & 0 & 0 & -96 & -12L & 120 & -6L & -24 \\ 0 & 0 & 0 & 12L & L^2 & -6L & \frac{7L^2}{2} & -6L \\ 0 & 0 & 0 & 0 & 0 & -24 & -6L & 24+\frac{K_2L^3}{EI} \end{bmatrix} \begin{Bmatrix} rs_1 \\ rb_1 \\ \alpha b_1 \\ r\,\mathrm{im}_1 \\ \alpha\,\mathrm{im}_1 \\ rb_2 \\ \alpha b_2 \\ rs_2 \end{Bmatrix} = \begin{Bmatrix} 0 \\ 0 \\ 0 \\ 0 \\ 0 \\ 0 \\ 0 \\ 0 \end{Bmatrix} \quad (55)$$

Fig. 5a shows that the stability in the neighborhood of the equilibrium position is guaranteed when the rotating speed ω is greater than the first natural frequency ω_1 of the rotating shaft. However, it seems that the other natural frequencies ω_2, ω_3 and … are irrelevant to the stability of the system. Fig. 5b shows the effect of the fluid damping on the stability of the system. Obviously, it shows that the system is not able to achieve the partial balancing if $D = 0$. This means that the fluid damping D is an important factor for balancing.

5. Time responses

Time responses of the given system are investigated to verify the stability of the system and to analyze the dynamic behavior. From the nonlinear equations of motion obtained from Eq. (32), the time responses are computed by the generalized-α time integration method [23]. When the number of ball-balancers and unbalanced masses are 2 and 1, respectively, i.e., $n = 2$ and $q = 1$, the nonlinear equations may be expressed by the relations (34) and (35). Note that in the relations (34) and (35) the mass matrix $\mathbf{M}$ is a function of the displacement vector $\mathbf{x}$ while the internal force vector $\mathbf{N}$ is a function of the displacement vector $\mathbf{x}$ and the velocity vector $\dot{\mathbf{x}}$. The material properties and dimensions for computation of time responses are given in Table 1. The mass moments of inertia Jb_i and JZb_i are given by Eq. (50). Time responses are computed for

two cases. First the system without balls is considered and finally the dynamic analysis is done for the same system equipped with two ball-balancers. In these two cases, the angular velocity ratio, ω/ω_1, is 5 where ω_1 is the first natural frequency of the system. The initial conditions are given in Table 2.

Figs. 6a–c clearly show the unwanted vibrations for radial displacements rs_1, rb_1 and $r\,\mathrm{im}_1$, respectively. Obviously, the use of a balancing mechanism is necessary for minimizing the vibrations. This aim can be achieved employing the auto balancing technique.

Table 2
Initial values of parameters.

Parameter	Initial value at $t = 0$
rs_1 (mm)	0.00001
rb_1 (mm)	0.00001
αb_1 (deg)	0
βb_1(deg)	0
φ_{11} (deg)	0
φ_{12} (deg)	π
$r\,\mathrm{im}$ (mm)	0.00001
$\alpha\,\mathrm{im}$ (deg)	0
$\beta\,\mathrm{im}$ (deg)	0

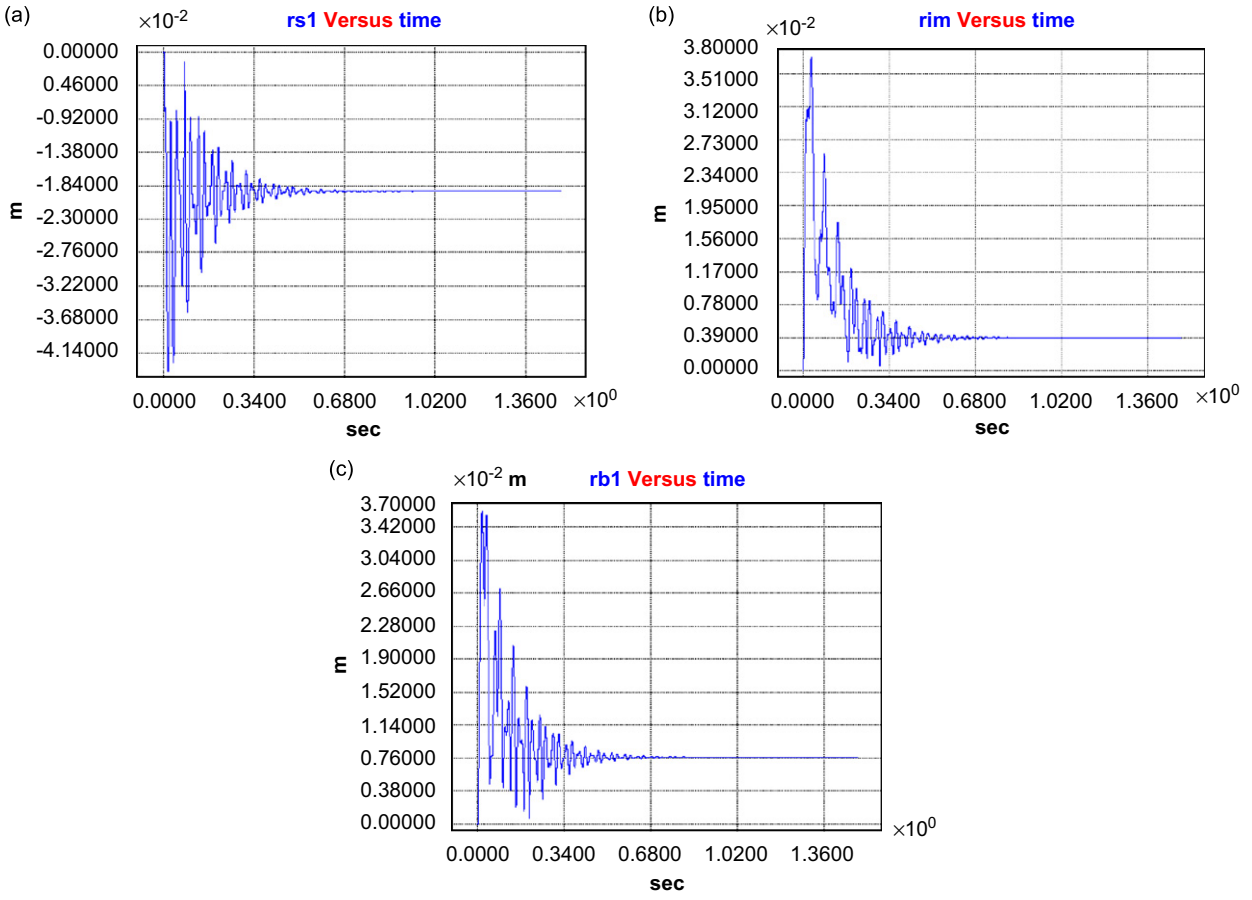

Fig. 6. Time responses of the system without balls when $\omega/\omega_1 = 5$: (a) the radial displacement, rs_1; (b) the radial displacement, $r\,\mathrm{im}_1$; (c) the radial displacement, rb_1.

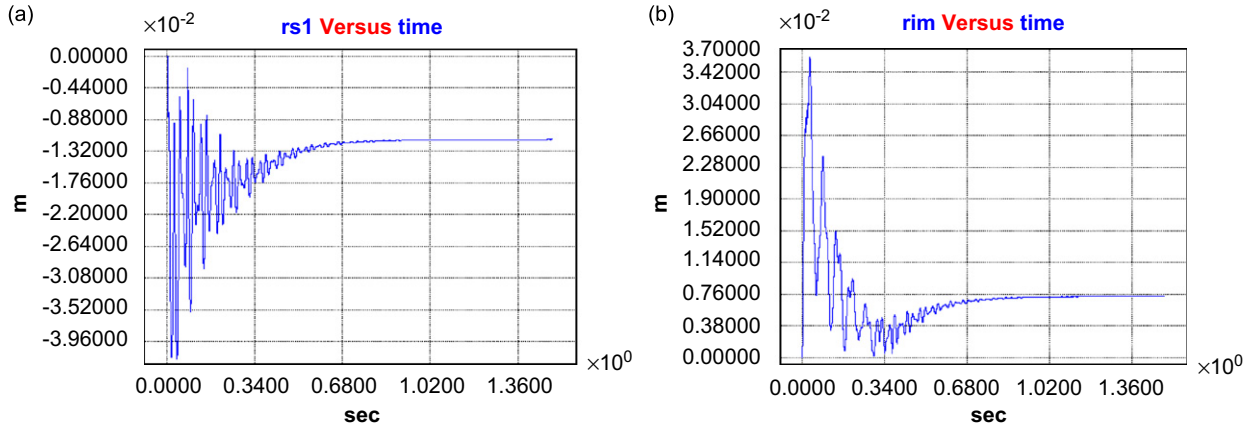

Fig. 7. Time responses of the first support position when $\omega/\omega_1 = 5$, the rest of the parameters are as Table 1: (a) the radial displacement, rs_1 (b) the radial displacement, $r\,\mathrm{im}_1$.

It must be noted that this method is not able to balance the system perfectly in all the cases. When the unbalanced point masses are in the planes of the auto ball-balancers, all the vibration amplitudes converge to zero, i.e., the perfect balancing. However, by using this method the vibration behavior of the system can be improved strongly. Figs. 7 and 8 show the time responses for a system equipped with two ABBs; material properties and geometric dimensions are given in Table 1.

Fig. 5 shows that the rotating speed $\omega/\omega_1 = 5$ is in the stable region; therefore, the ball-balancers perform their duty, i.e., minimizing the unwanted vibration of the system and Fig. 8 confirming the stability analysis. However, for rotating speeds of $\omega/\omega_1 \leqslant 1$ the auto ball-balancers do not have any positive effect on the improvement of the vibration behavior of the system.

Fig. 8b shows the time responses of the ball-positions for the first auto ball-balancer, because of the symmetry there is the same situation for the balls of the second auto ball-balancer. These two graphs show that the four balls of the auto ball-balancers are in the opposite side of the unbalanced mass and in the specified positions as Table 3.

Table 3 demonstrates the converged values of the variable parameters before and after auto balancing. As mentioned before, because of the symmetry of the system, only the results for the first auto ball-balancer and support have been presented.

A criterion is needed for doing a comparison between the vibration behaviors of the system without auto ball-balancers and equipped with the balancing instruments. For this reason, the summation of amplitude squares of rs_1, rb_1 and $r\,\mathrm{im}_1$ is considered as a target function. It is clear that smaller values of target function cause a better vibration behavior. Using the numerical results of Table 3, the values of the target function for the system with and without auto ball-balancers are 185.5 and 434.3, respectively. The reduction in the value of the target function from 434.3 to 185.5 shows a good improvement in the vibration behavior of the system.

Fig. 9 shows that the closer the ABBs are to the location of the unbalanced mass, the better vibration behavior of the system is, i.e., the value of the target function is smaller. Using Table 4, these values are 1492.5, 33.5 and 0 for the cases (a), (b) and (c) in Fig. 9, respectively. Figs. 9c and 10 indicate that if the unbalanced mass is in the planes of auto ball-balancers the perfect balancing is achieved, i.e., the value of the target function is zero. So, this figure indicates the importance of the ball-balancers' positions. It is clear that specifying the accurate positions of the imbalances in a system is not possible or at least is a difficult problem. However, using this balancing mechanism, we would be able to minimize the vibrations of the system without knowing the exact positions of the unbalanced masses.

6. Conclusions

In this paper, dynamic stability and time responses are analyzed for a system of unbalanced flexible rotating shaft equipped with n automatic balancers. Also, the system lies on two linear elastic supports. This study

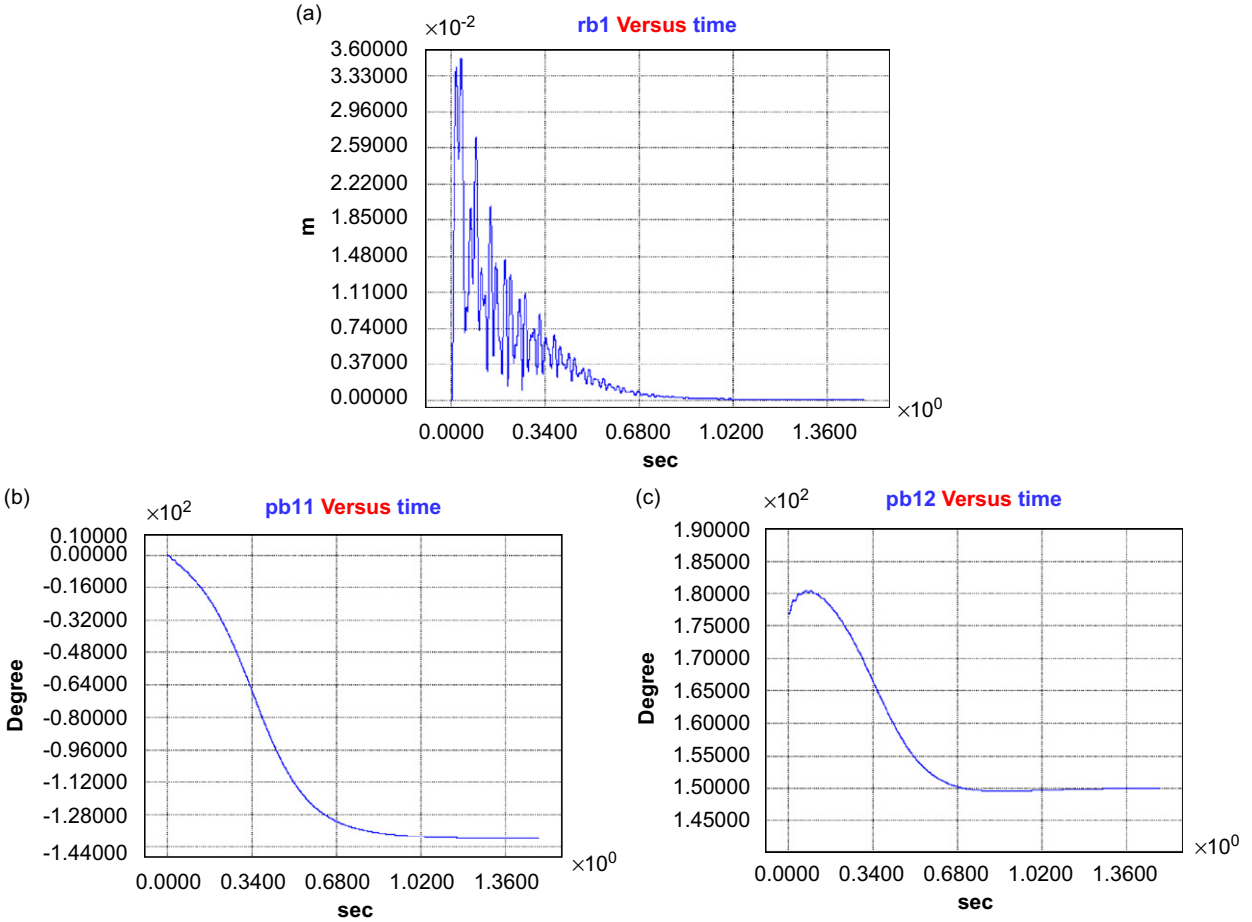

Fig. 8. Time responses of the automatic ball-balancers when $\omega/\omega_1 = 5$, the rest of the parameters are as Table 1: (a) the radial displacement, rb_1; (b) the ball positions ϕ_{11}, ϕ_{12}.

Table 3
Converged values of variable parameters before and after auto balancing, the material properties and dimensions for computation of time responses are given by Table 1.

Parameter	Converged values before auto balancing	Converged values after auto balancing
rs_1 (mm)	−18.98	−11.5
rb_1 (mm)	7.7	0.045
φ_{11} (deg)	–	−139
φ_{12} (deg)	–	152
r im (mm)	3.84	7.3

adopts the Stodola–Green rotor model to consider the rigid-body rotations due to shaft flexibility instead of Jeffcott rotor model. The nonlinear equations of motion are derived for an autonomous system considering the ball-balancer of Stodola–Green rotor, utilizing the perturbation method, an equilibrium position and the linearized equations are obtained. Furthermore, the stability analysis is performed using the Routh–Hurwitz criteria. Moreover, time responses are investigated for the nonlinear

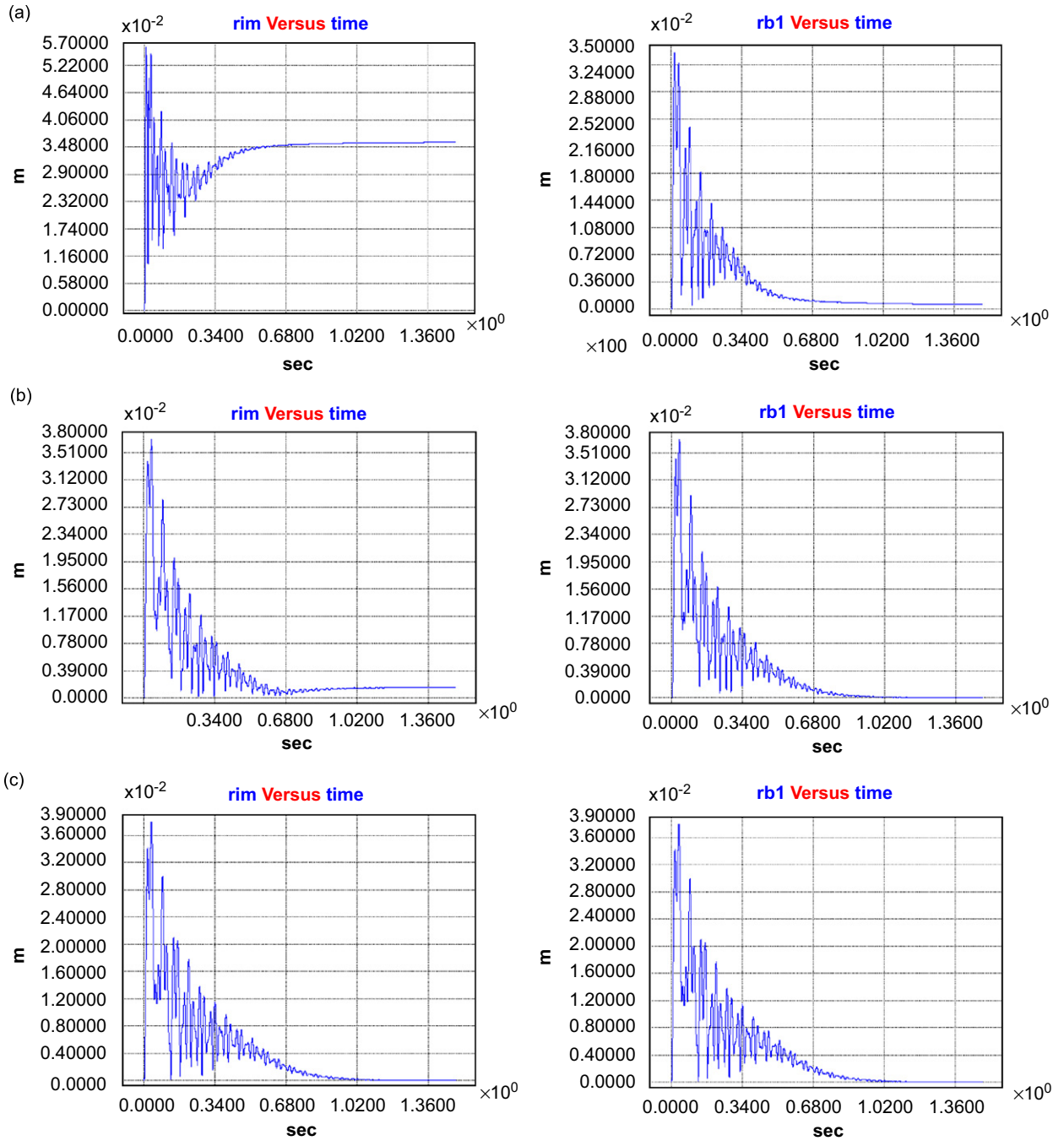

Fig. 9. Time responses of the radial displacements of the unbalanced mass and the automatic ball-balancers when $\omega/\omega_1 = 5$: (a) $zb_1 = 0.2$, $zb_2 = 1.8$; (b) $zb_1 = 0.7$, $zb_2 = 1.3$; (c) $zb_1 = zb_2 = 1$.

equations of motion using the generalized-α method. The results of this study may be summarized as follows:

(1) To obtain the partial balancing, the rotating speed should be more than the first natural frequency.
(2) The auto ball-balancers tend to minimize the vibration behavior only in the case of which the system parameters are in the stability region for the equilibrium position.

Table 4
Converged values of the variable parameters after auto balancing, the material properties and dimensions for computation of time responses are given by Table 1.

Parameter	Converged values before auto balancing $zb_1 = 0.2$, $zb_2 = 1.8$	Converged values after auto balancing $zb_1 = 0.7$, $zb_2 = 1.3$	Converged values after auto balancing $zb_1 = zb_2 = 1$
rs_1 (mm)	−14	−5.6	0
rb_1 (mm)	0.65	0.0082	0
φ_{11} (deg)	−155.7	−138.94	−140.8
φ_{12} (deg)	168.4	145.84	141
r im (mm)	36	1.47	0

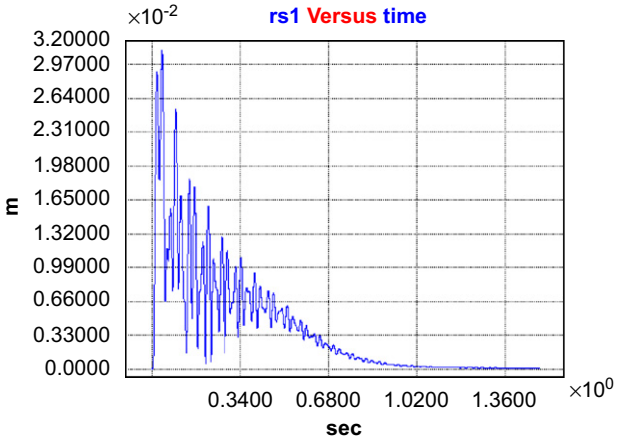

Fig. 10. Time response of the radial displacement of the first support when $\omega/\omega_1 = 5$, $zb_1 = zb_2 = 1$.

(3) Closer distance between auto ball-balancers and unbalance masses leads to better vibration behavior of the system.
(4) The complete balancing is obtained when all the unbalanced masses are in the planes of the auto ball-balancers.
(5) The fluid damping coefficient D is one of the essential parameters to gain balancing.

References

[1] E.L. Thearle, Automatic dynamic balancers (Part 1. Leblanc balancer), *Machine Design* 22 (1950) 119–124.
[2] E.L. Thearle, Automatic dynamic balancers (Part 2. Ring, pendulum, ball balancers), *Machine Design* 22 (1950) 103–106.
[3] J.D. Alexander, An automatic dynamic balancer, *Proceeding of the 2nd Southeastern Conference*, Vol. 2, 1964, pp. 415–426.
[4] J.W. Cade, Self-compensating balancing in rotating mechanisms, *Design News* (1965) 234–239.
[5] J. Adolfsson, A Study of Stability in Auto Balancing Systems Using Multiple Correction Masses, Licentiate Thesis, Department of Mechanics, Royal Institute of Technology, S-100 44 Stockholm, Sweden.
[6] J. Lee, An analytical study of self-compensating dynamic balancer with damping fluid and ball, *Shock and Vibration* 2 (1995) 59–67.
[7] J. Lee, W.K. Van Moorhem, Analytical and experimental analysis of a self-compensating dynamic balancer in a rotating mechanism, *ASME Journal of Dynamic Systems, Measurement, and Control* 118 (1996) 468–475.
[8] J. Chung, D.S. Ro, Dynamic analysis of an automatic dynamic balancer for rotating mechanisms, *Journal of Sound and Vibration* 5 (1999) 1035–1056.
[9] C.H. Hwang, J. Chung, Dynamic analysis of an automatic ball-balancer with double race, *JSME International Journal Series C* 42 (1999) 265–272.
[10] L. Sperling, B. Ryzhik, Ch. Linz, H. Duckstein, Simulation of two-plane automatic balancing of a rigid rotor, *Mathematics and Computers in Simulation* 58 (2002) 351–365.

[11] J. Chung, I. Jang, Dynamic response and stability analysis of an automatic ball balancer for a flexible rotor, *Journal of Sound and Vibration* 1 (2003) 31–43.
[12] P.C.P. Chao, Y.D. Huang, C.K. Sung, Non-planar dynamic modeling for the optical disk drive spindles equipped with an automatic balancer, *Mechanism and Machine Theory* 38 (11) (2003) 1289–1305.
[13] Q. Yang, E.H. Ong, J. Sun, G. Guo, S.P. Lim, Study on the influence of friction in an automatic ball balancing system, *Journal of Sound and Vibration* 285 (1–2) (2005) 73–99.
[14] W. Kim, D.J. Lee, J. Chung, Three-dimensional modeling and dynamic analysis of an automatic ball balancer in an optical disk drive, *Journal of Sound and Vibration* 285 (3,22) (2005) 547–569.
[15] C. Rajalingham, R.B. Bhat, Complete balancing of a disk mounted on a vertical cantilever shaft using a two ball automatic balancer, *Journal of Sound and Vibration* 290 (1–2, 21) (2006) 169–191.
[16] K. Green, A.R. Champneys, N.J. Lieven, Bifurcation analysis of an automatic dynamic balancing mechanism for eccentric rotors, *Journal of Sound and Vibration* 291 (3–5) (2006) 861–888.
[17] C.J. Lu, C.H. Hung, Stability analysis of a three-ball automatic balancer, *Journal of Vibration and Acoustics* 130 (5) (2008) 051008.
[18] C.C. Cheng, F.T. Wu, K.S. Hsu, K.L. Ho, Design and analysis of auto-balancer of an optical disk drive using speed-dependent vibration absorbers, *Journal of Sound and Vibration* 311 (1–2) (2008) 200–211.
[19] D.J. Rodrigues, A.R. Champneys, M.I. Friswell, R.E. Wilson, Automatic two-plane balancing for rigid rotors, *International Journal of Non-Linear Mechanics* 43 (6) (2008) 527–541.
[20] D. Childs, *Turbo machinery Rotor Dynamics: Phenomena, Modeling, and Analysis*, Wiley, New York, 1993.
[21] A. Stodola, *Steam and Gas Turbines*, McGraw-Hill, New York, 1927.
[22] R. Green, Gyroscopic effects of the critical speeds of flexible rotors, *ASME Journal of Applied Mechanics* 15 (1948) 369–376.
[23] J. Chung, G.M. Hilbert, A time integration algorithm for structural dynamics with improved numerical dissipation: The generalized-α method, *ASME Journal of Applied mechanics* 60 (1993) 371–375.